LWT - Food Science and Technology 84 (2017) 520–528

Contents lists available at ScienceDirect

LWT - Food Science and Technology

journal homepage: www.elsevier.com/locate/lwt

Influence of extrusion process conditions on starch film morphology

Paula González-Seligra [a], Lucas Guz [a, b], Oswaldo Ochoa-Yepes [a], Silvia Goyanes [a, **], Lucía Famá [a, *]

[a] Universidad de Buenos Aires, Facultad de Ciencias Exactas y Naturales, Departamento de Física, Laboratorio de Polímeros y Materiales Compuestos (LPM&C), Instituto de Física de Buenos Aires (IFIBA-CONICET), Ciudad Universitaria (1428), Ciudad Autónoma de Buenos Aires, Argentina
[b] Instituto de Investigación e Ingeniería Ambiental, CONICET, Universidad Nacional de San Martín, 25 de Mayo y Francia (1650), San Martín, Provincia de Buenos Aires, Argentina

ARTICLE INFO

Article history:
Received 8 February 2017
Received in revised form
9 June 2017
Accepted 12 June 2017
Available online 13 June 2017

Keywords:
Extrusion process conditions
Screw speed
Starch
Morphology
Physicochemical properties

ABSTRACT

The conditions of extrusion process for food packaging are determinant on their morphology and, as consequence, on their functionality. The effect of the screw speed of a starch-glycerol system extruded at the same temperature profile was evaluated. The process at 80 rpm led to a material with the starch completely gelatinized, while the systems fabricated at 40 rpm and 120 rpm presented broken starch grains. The morphology and density of the broken grains depended on the screw speed. The material at 120 rpm showed broken grains with smaller size and lower concentration than that observed in the system at 40 rpm. After pressing at 120 rpm, the film formed (TPS120) resulted similar than that at 80 rpm (TPS80), while the film at 40 rpm (TPS40) kept some broken grains. TGA of the material obtained at 40 rpm showed more than one degradation process of the glycerol due to the inhomogeneous glycerol dispersion. DRX revealed more cristallinity in TPS40, being TPS120 the most amorphous. TPS80 had the highest strain at break while the others the higher modulus and stress at break. Water vapor permeability of TPS80 and TPS120 showed similar results and lower than TPS40.

1. Introduction

New trends have focused on the use of biodegradable, non-toxic and edible films based on polymers as packaging to retard the deleterious effects of food, decrease waste from plastics and reduce costs (Bashir, Swer, Prakash, & Aggarwal, 2017; Brand-Williams, Cuvelier, & Berset, 1995; Campos-Requena, Rivas, Pérez, Garrido-Miranda, & Pereira, 2015; Famá, Bittante, Sobral, Goyanes, & Gerschenson, 2010; Jaramillo, Gutiérrez, Goyanes, Bernal, & Famá, 2016; Moreno et al., 2014). Particularly, the low costs of starch and the great source of production make it very promising for its implementation as polymer-base of biodegradable materials in food packaging markets (Goudarzi, Shahabi-Ghahfarrokhi, & Babaei-Ghazvini, 2017; Homayouni, Kavoosi, & Nassiri, 2017). One of the major problem to implement these materials on the market is the poor knowledge of plastics companies about the possible production of large-scale starch-based thermoplastic products without having to invest in new equipment. This is because most research related to the production of biodegradable starch films use casting technique (Famá, Pettarin, Goyanes, & Bernal, 2011; Kibar & Us, 2013; Piñeros-Hernandez, Medina-Jaramillo, López-Córdoba, & Goyanes, 2017; Wang et al., 2017). Such method consists in small quantities and large time process, then, it is not the best to large-scale production of films, therefore limiting their industrial application. Considering this, it is imminent to launch the development of thermoplastic starch materials by the processes with the standard equipment used in the manufacture of synthetic polymers, such as extrusion. Processing of starch by this technique has great advantages due its excellent mixing capacity, operational flexibility and its low infrastructure cost. However, it has been little investigated probably because starch extrusion process is more complex than other polymers, due to starch multiphase transitions during thermal processing as gelatinization, granule expansion, melting, decomposition and recrystallization (Borries-Medrano, Jaime-Fonseca, & Aguilar-Mendez, 2016; Li et al., 2011; Xie et al., 2016). Extrusion implicates both thermal and mechanical energy (Alam, Pathania, & Sharma, 2016; Ghanbarzadeh & Almasi, 2013). During this process, starch is subjected to relatively high pressure, heat,

* Corresponding author.
** Corresponding author.
E-mail addresses: pseligra@df.uba.ar (P. González-Seligra), guzlucas@df.uba.ar (L. Guz), oswaldo@df.uba.ar (O. Ochoa-Yepes), goyanes@df.uba.ar (S. Goyanes), merfama@hotmail.com, lfama@df.uba.ar (L. Famá).

http://dx.doi.org/10.1016/j.lwt.2017.06.027
0023-6438/

and mechanical shear forces that produce multiple chemical and physical reactions and crystalline structure of the starch granules is destroyed. In the presence of a plasticizer, starch granular structure is disrupted and converted into a thermoplastic starch (TPS) (Graaf, Karman, & Janssen, 2003; Kruiskamp, Smits, Van Soest, & Vliegenthart, 2001). During the extrusion starch based materials undergoes marked thermo-mechanical transformations surely leading to significant changes in their physicochemical properties (Deng et al., 2014; Hietala, Mathew, & Oksman, 2013; Rosa et al., 2008). Operating conditions, such temperature profile and screw speed, have several influence on mechanical disruption and starch transformation (Lai & Kokini, 1991; Zepon, Vieira, Soldi, Salmoria, & Kanis, 2013). One of the most important parameters that influence starch reactions in the extrusion process is the specific mechanical energy (SME). SME is the amount of mechanical energy (work) dissipated as heat inside the material, expressed per unit mass of the material (Godavarti & Karwe, 1997). According to García (García, Famá, D'Accorso, & Goyanes, 2015), SME can be calculated using the following equation:

$$SME = \frac{P \times \tau \times \frac{RPM_{act}}{RPM_{rated}}}{\dot{m}} \quad (1)$$

where P is the motor power, expressed in kW, τ is the difference between the running torque and the torque when the extruder is running empty divided by the maximum allowable torque, RPM_{act} is the actual screw rpm, RPM_{rated} is the maximum allowable screw rpm, $\dot{m}$ is the mass flow rate of the system (kg/sec).

In the case of thermoplastic starch systems, if SME is low, the amount of mechanical energy may be not enough to broken starch grains and efficiently complete the extrusion process. The effect of screw speed on SME was studies by different authors (Chaudhary, Miler, Torley, Sopade, & Halley, 2008; Oniszczuk et al., 2015). In particular, Oniszczuk (Oniszczuk et al., 2015) processed corn starch using a single screw extruder at 60, 80 and 100 rpm and they observed an increase in SME when screw speed was growing.

As can be seen in eq. (1), the screw speed of the process plays a relevant role in the specific mechanical energy and therefore in final properties of the extruded films. At low RPM_{act} values, SME may not be sufficient to achieve a successful process of TPS. Li (Li et al., 2011) investigated the effects of starch materials with different amylose/amylopectin ratios on processibility and film performance. The authors studied the effect of screw speed on the torque, showing that for speeds screw above 120 rpm very unstable torque was produce and unsteady extruded flow at the die outlet. It is important to note that the influence of screw speed on final properties of the films were not analyzed in the work of Li (Li et al., 2011). The choice of screw speed most of the time depends on the type of starch and plasticizer used to be processed (Deng et al., 2014; Kelly, Brown, & Coates, 2006). Some studies on the transformation of starch suggested that intense shear fields within the extruder caused mechanical disruption and thus loss of crystallinity (Lai & Kokini, 1990, 1991; Liu, Xie, Yu, Chen, & Li, 2009).

To date, there are only few published studies on extrusion processing of thermoplastic starch. In particular, there are not researches about the effect of the speed screw of the process and its consequence in the final properties of starch materials. The knowledge of the correct values of the parameters involved in the process of extrusion of a material with possibilities to be in food packaging market is crucial to obtain a final product with the appropriate characteristics according to its use.

Considering the importance to promote the use of biodegradable materials as packing, employing the same technology used for synthetic polymers like extrusion, the aim of this investigation is to evaluate one of the most important parameter of this process, speed screw, from the extrusion of starch, glycerol and water at different rpm. It want to demonstrate the ease of implementing biodegradable packaging from starch in the market, using actual machinery, facilitating its process and decreasing industrial sector inversion.

2. Experimental

2.1. Materials

Commercially available cassava starch (amylose 18 g/100 g of starch and amylopectin 82 g/100 g of starch) was supplied by CODIPSA (Asunción, Paraguay) and glycerol was of analytical grade (Aldrich, Buenos Aires, Argentina).

2.2. Process conditions and films preparation

All materials were prepared by extrusion technique using a co-rotating twin screw extruder (Nanjing Kerke Extrusion equipment Co., Ltd., Jiangsu, China) with screw diameter (D) of 16 mm and length to diameter ratio L/D = 40. The equipment consists in two parallel screw shafts that either rotate in the same direction (co-rotating). There are ten temperature-controlling zones along the barrel of the extruder equipped with a cylindrical die of 4 mm (Fig. 1a). The effect of extrusion screw speed on the processibility of starch was studied by using three different the screw speeds: 40 rpm, 80 rpm and 120 rpm (with feeding rates of 6 g/min, 12 g/min and 15 g/min, respectively), while keeping the temperature profile of extrusion process. Considering the thermal process of starch, the selected temperature profile used was: 90°C/100°C/110°C/120°C/120°C/130°C/130°C/140°C/130°C/120 °C (from the feeder to the die).

Thermoplastic starch threads (T) and films (TPS) were developed by the same components and quantities in order to evaluated the effect of the process condition. Cassava starch (60 g/100 g of system) was incorporated to a mixture of glycerol (20 g/100 g of system) and distillated water (20 g/100 g of system), then, the system was manually mixed until complete absorption of the liquid phase into the starch. After that, it was sieved with a mesh size of 2 mm and stored 24 h in sealed containers according with Wang (Wang & Ryu, 2013) before extrusion. The mixture was process using the mentioned a temperature profile and the different screw speeds. After processing, three different threads, one of each screw speed used, were obtained (Fig. 1b), stabilized for 4 weeks in a conditioned chamber at 56% RH (saturated NaBr). (Famá, Goyanes, & Gerschenson, 2007). Then, pellets from each system were obtained by the pelletization of the threads using an automatic pelletizer (Weinuo Technology Co., Ltd, Jiangsu, China). TPS films were prepared by thermo-compression using a thermostatized hydraulic press following the procedure of Gilfillan (Gilfillan, Moghaddam, Bartley, & Doherty, 2016). Pellets (~4 g) were placed between Teflon sheets in the press and heated to 140 °C for 15 min. At that moment, it increased the pressure to 56 kPa and decreased the temperature up to ~40 °C. The resultant films (TPS40, TPS80 and TPS120), with thickness of approximately 0.3 mm, were conditioned at 56% RH before tested.

3. Characterization

3.1. Scanning electron microscopy (SEM)

The morphology of the cryogenic fracture surface of both thread and films were tested by field emission SEM (FE-SEM) using a Zeiss DSM982 Gemini (Oberkochen, Germany) with a field emission gun equipment. Cryogenic fractured samples were previously coated

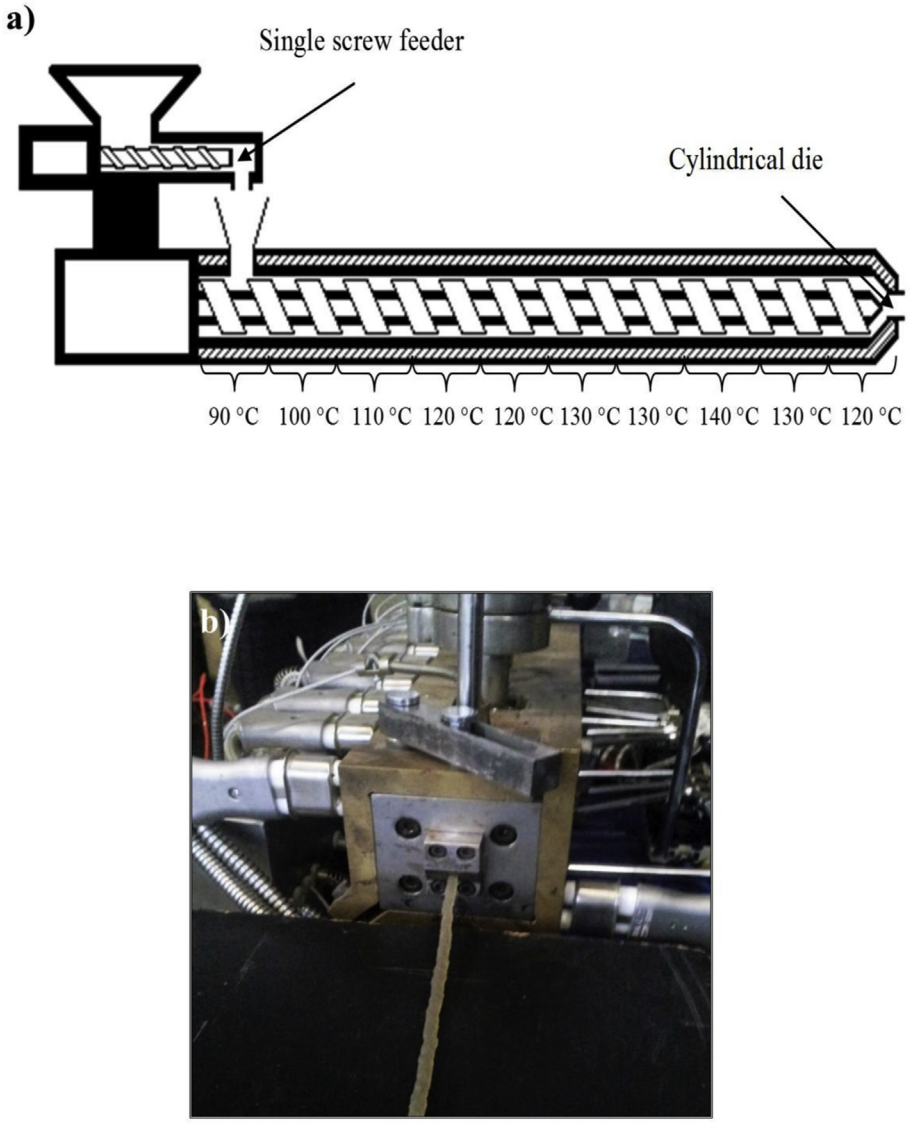

Fig. 1. (a) Scheme of the extruder used for the threads developed, equipped with ten heating zones plus a cylindrical die of 4 mm, and (b). The resultant thread after processing.

with platinum using a vacuum sputter coater and then observed at magnifications of 1000× and 5000X.

3.2. Thermal characterization (TGA/DTA)

A simultaneous thermogravimetric/differential thermal analyzer (TGA/DTADTG-60 Shimadzu instrument, Kyoto, Japan) was used to evaluate the thermal stability of the threads and films. Approximately 10 mg of sample was subjected to heating from 30 °C to 500 °C at a rate of 10°C/min in a dry nitrogen atmosphere and flow rate of nitrogen of 30 mL/min. Thermogravimetric behavior of the threads was evaluated from the curves of TGA and thermal properties of films were analyzed by TGA and DTA. Assays were performed in triplicate. The standard error in each system was less than 1%. The representative curves of each system were reported.

3.3. X-ray diffraction (XRD)

The X-ray diffraction patterns of the films were measured with a Siemens D 5000 X-ray diffractometer, Texas, USA (Cu Kα radiation and wavelength of 1.54 Å). Operation was performed at tension of 40 kV and current of 30 mA. Data were collected with a scintillation counter in a scattering angle 2θ in the range of 5–35° with a step size of 0.02°. Three replicates were tested for each system. Standar error was of 2%. Representative curve was presented for each system.

3.4. Mechanical properties (DMTA)

Mechanical characterizations (uniaxial tensile and dynamic tests) of the films were performed using a dynamic mechanical thermal analyzer (DMTA IV, Rheometric Scientific, New jersey, USA). Dynamic mechanical measurements were carried out in the rectangular tension mode at 1 Hz and a heating rate of 2°C/min. The temperature range of measurements was from room temperature (25 °C) to 120 °C. The strain amplitude was 0.1% to assure that the mechanical response of the samples was within the linear visco-elastic range (Famá, Rojas, Goyanes, & Gerschenson, 2005). Sample dimensions were 16.0 mm × 4.8 mm x 0.30 mm (length, width and thickness, respectively). Transition processes were analyzer by the loss tangent dependence on temperature curves. Three replicates

were tested for each system. Standard error was 1%. Representative curve was presented for each system.

Quasi-static tests at 1 Hz and 25 °C. Stress (σ)-strain (ε) curves were obtained and evaluated to determine Young's modulus (E), stress at break (σ_b) and strain at break ($\varepsilon;_b$) parameters. Pieces of the film for quasi-static assays were cut according to Famá et al. (2005), resulting 10.0 mm × 4.8 mm x 0.30 mm (effective length, width and thickness). The reported values of the different parameters are the average of at least 12 measurements. Standard error was 15%. Representative curve was presented for each system.

3.5. Water solubility (S)

Water solubility of films (S) was determined following Maizura (Maizura, Fazilah, Norziah, & Karim, 2007). Film samples (~0.5 g) were dried at 50 °C for 24 h and then, they were weighed (m_{si}) and placed in beakers with 100 mL of distillate water for 24 h at room temperature (25 °C). Film remnants were separated by filtration and dried at 50 °C to constant weight (24 h in all cases) (m_{sf}). Experiments were run in triplicate and the percentage of total soluble mass was calculated as:

$$S = \frac{\left(m_{si} - m_{sf}\right)}{m_{si}} \times 100 \quad (2)$$

3.6. Water vapor permeability (WVP)

Water vapor permeability (WVP) of the different films was determined at room temperature (25 °C) using a modified ASTM E96-00 procedure (Famá, Rojo, Bernal, & Goyanes, 2012). Samples were placed into circular acrylic cells containing $CaCl_2$, and located in desiccators at RH of ~70% (NaCl). Water vapor transport through the films (WVT) was determined from the rate of the weight increment of the system in the time, measuring over 24 h for 10 consecutive days. Finally, WVP were calculated as:

$$WVP = \frac{WVT \times e}{P_0 \times RH} \quad (3)$$

Where e is the film thickness and P_0 is the saturation vapor pressure of water at room temperature.

4. Results and discussions

Cryogenic fractured surface micrographs of the three threads obtained by extrusion and stabilized for 4 weeks, before being pelletized (T40, T80 and T120), are showed in Fig. 2. The samples processed at 40 rpm and 120 rpm presented broken starch grains into a smooth surface, consequence of the presence of starch grains, which cause crack propagations leading to that type of surface. In T80 a homogeneous rough surface without grains as typical starch materials plasticized with glycerol was observed. The size and density of broken starch grains in T120 resulted smaller than in T40.

The extrusion process of starch-plasticizer involves both chemical and physical reactions, e.g. granule expansion, gelatinization, decomposition, melting and crystallization (Lai & Kokini, 1991; Liu et al., 2009). If the energy involved in the process is not enough, it is possible that some of starch grains do not reach to break. T40 showed higher amount of whole starch grains (Fig. 2a), indicating that the specific mechanical energy (SME) was not enough to break some starch grains. SME is proportional to screw rpm (eq (1)) then lower rpm means less of this parameter. Taking into account SEM micrograph of T40, it can concluded that 40 rpm

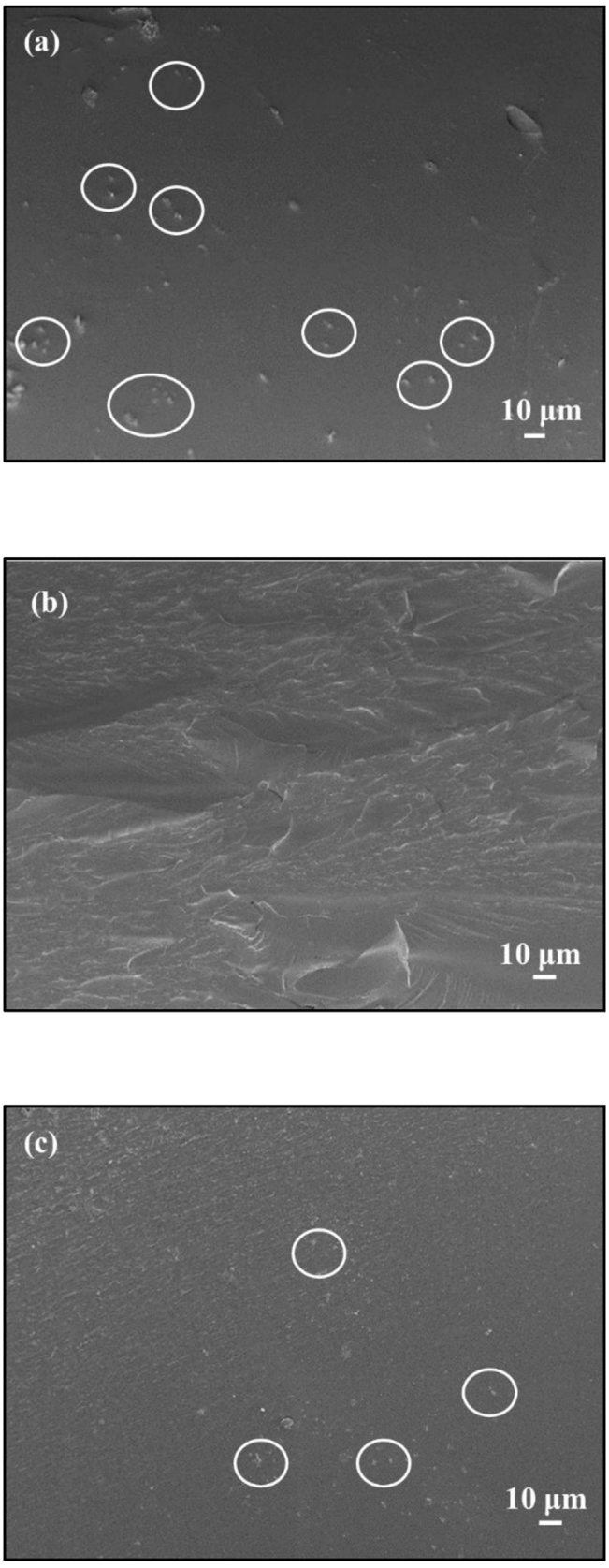

Fig. 2. FE-SEM micrograph of the cryogenic fracture surface of (a) T40, (b) T80, and (c) T120. Magnification of 1000 X. Circles shows the presence of starch grains in T40 and T120.

was not enough to process our material. In the case of the thread fabricated at 80 rpm, SME seemed to be sufficient to obtain a plasticized material without the presence of grains (Fig. 2b).

When rpm increased to 120, according to eq (1), SME also increased leading to a higher process energy than T40 and T80. In this context, non-presence of grains would have been expected in T120; however, some broken grains are observed (although smaller but at lower density than in T40), demonstrating that part of the material at 120 rpm did not fully processed. It is well known that starch gelatinization in extrusion also involves temperature and time (Lai & Kokini, 1991). If the extrusion process takes place in a short time, total gelatinization of starch may not occur. Taking this into account, and that the temperature profile was similar in all cases, the presence of grains in T120 is due to the short time elapsed during the process.

Then, screw speed of 80 rpm is the most optimal in terms of mechanical shear forces and processing time to obtain plasticized starch materials fully gelatinized.

Cryogenic fractured surface of the films was also evaluated in order to observe the differences between the material before and after pressing. The micrographs of the different thermoplastic starch films (TPS40, TPS80 and TPS120) are exposed in Fig. 3. The film processed at 80 rpm conserved the rough surface showed in the thread (T80). On the other hand, TPS40 conserved part of the grains observed in the threads extruded at that rpm (T40). A notorious change occurred in the material processed at 120 rpm when it was pressing since broken starch grains disappeared (Fig. 3c). This is because during the pressing process, the grains completed the gelatinization and/or melted by the pressure/temperature/time used. Then, TPS120 finally resulted a material without grain after pressing for the formation of a film. These results are very relevant considering the use that it want it give. If it is to be used as a film, the process at 120 rpm leads to a thermoplastic starch material with homogeneously distributed glycerol, while as thread will have an inhomogeneous material.

Thermal behavior of the different threads obtained after extrusion (T40, T80 and T120) is shown in Fig. 4a. All thermograms revealed three step degradation processes, typical of starch films with glycerol (Gutiérrez, Morales, Pérez, Tapia, & Famá, 2015; Jaramillo et al., 2016; Saiah et al., 2009).

The first zone, between 100 and 150 °C, corresponds to water and/or volatiles evaporation. The second stage is related to the decomposition of glycerol-rich phase, which occurs between 180 and 280 °C. The last and main degradation stage at around 280–350 °C is attributed to starch degradation (García, Famá, Dufresne, Aranguren, & Goyanes, 2009; Rodríguez-Castellanos, Martínez-Bustos, Rodrigue, & Trujillo-Barragán, 2015). The thread processed at 40 rpm presents two marked mass loss in the region corresponding to the glycerol degradation, one strong at around 180 °C and the other around 220 °C. As it was shown in SEM image (Fig. 2a), T40 contains high amount of ungelatinized starch grains within a plasticized matrix. Plasticized zone concentrated all glycerol so it is feasible that more glycerol molecules were available to evaporate; then, higher mass loss in that stage was expectable. On the other hand, the inhomogeneity of glycerol dispersion in thread produced at 40 rpm led to the existence of more than one degradation process in that temperature range. This last behavior did not was observed in either T80, due to the homogeneous distribution of glycerol, or T120, probably due to the smaller density of ungelatinized grains presented in that material compared with T40, as it was shown in SEM micrographs (Fig. 2a and **c**). Screw speed variation did not affect starch degradation temperature of the threads (280–350 °C) because all extruded materials were developed from the same type and amount of starch.

TGA of films are exposed in Fig. 4b. Similar behavior of the thread at 40 rpm is observed for TPS40, while TPS80 y TPS120 showed the same mass loss behavior in the zone corresponding to

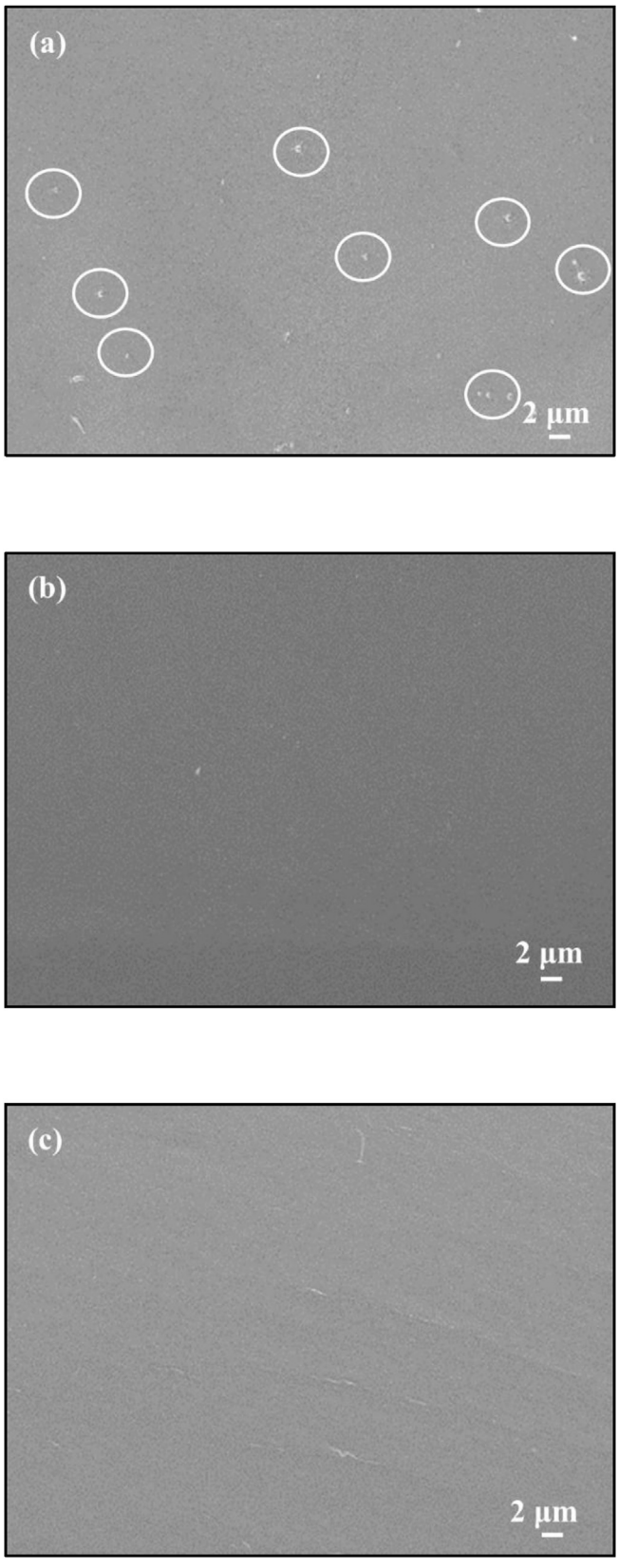

Fig. 3. FE-SEM micrograph of the cryogenic fracture surface of (a) TPS40, (b) TPS80 and (c) TPS120. Magnification of 5000 X. Circles shows the presence of starch grains in TPS40.

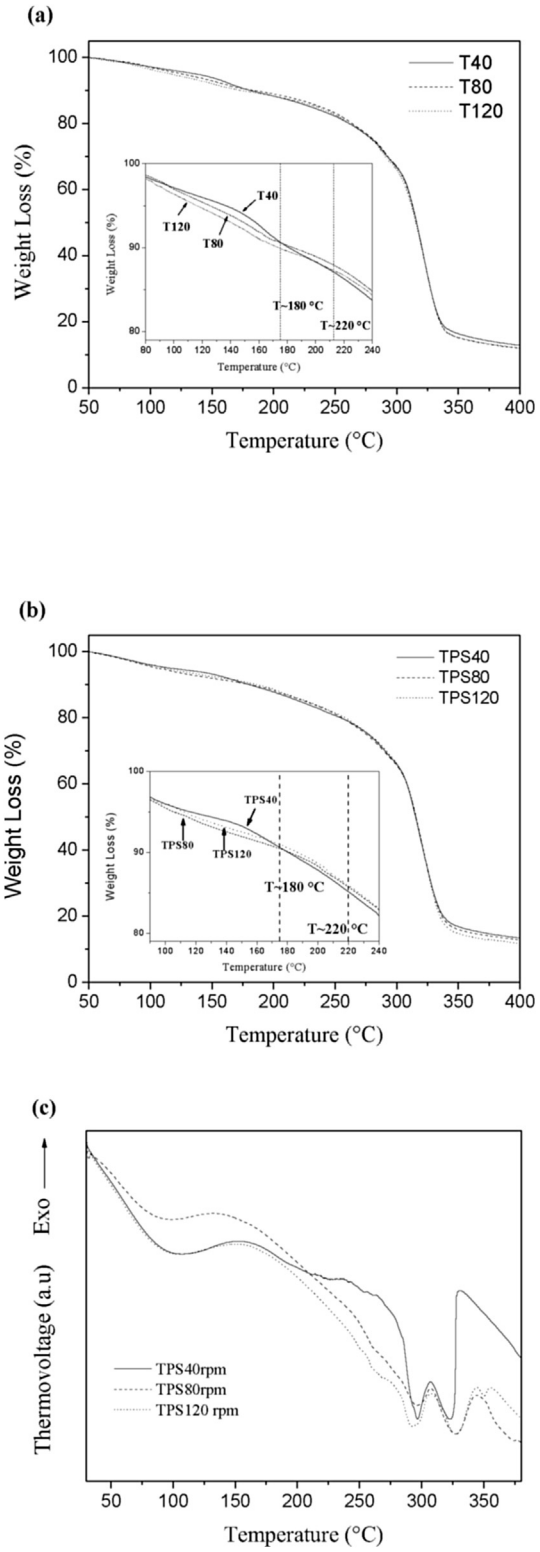

Fig. 4. Representative Weight Loss curves of (a) threads obtained at different rpm, (b) films obtained at different rpm, (vertical dash lines in the inserts show mass loss corresponding to glycerol degradation) and (c) differential thermal analysis (DTA). Representative curves for all films developed. The curves differ from each other by less than 1%.

glycerol degradation. TPS40 presents phase separation between glycerol and starch, indicating that in this systems, glycerol should be more available and then easier to thermal degrade. Finally, pressing process did not affect the starch degradation temperature of the films, resulting thermally stables up to temperatures around 280°C.

DTA curves of the different films are shown in Fig. 4c. In all films three endothermic processes it can be observed. The first, in the temperature range from 50 °C to 140 °C, is associated to the complete starch gelatinization of films once they were heated, and the others two, are related to the starch degradation. Starch endothermic process occurred in two consecutive steps corresponding to thermal decomposition of amylose (T ~ 295 °C) and amylopectin (T ~ 325 °C) (González-Seligra, Eloy-Moura, Famá, Druzian, & Goyanes, 2016).

TPS40 and TPS120 showed complete gelatinization peak at the same temperature (around ~ 103 °C), whereas TPS80 exhibited this peak at lower temperature (~95 °C) and with less intensity. As it was previously explained, the film processed at 80 rpm was a thermoplastic material with great glycerol distribution; therefore, it is expectable that this material need less temperature to complete its gelatinization (Li et al., 2011).

The presence of starch grains in TPS40 led to two well marked peaks related to amylose and amylopectin degradation, in contrast with TPS80 and TPS120, which showed smoother peaks due to the absence of grains in these films.

X-ray diffraction patterns (XRD) curves of the different studied films are presented in Fig. 5. As can be observed, TPS40 exhibits two peaks at $2\Theta = 12.9°$ and 19.6°. It is well known that during extrusion crystalline structure of starch granules is destroyed. However, in presence of plasticizers or lipids, amylose shows a unique capacity to form complexes with such small molecules, identified as V_H, V_A, and E_H-type crystals. The type of these structures depends on the extrusion parameters and starch composition (Van Soest, Hulleman, De Wit, & Vliegenthart, 1996). According Van Soest (Van Soest et al.,1996) at processing temperatures below 180 °C, V_H structure is favored. The two peaks of TPS40 that correspond to V_H-type crystals (Morales, Candal, Famá, Goyanes, & Rubiolo, 2015) are due to the formation of amylose-glycerol complex. Considering that the high density of broken starch grains in TPS40 (Fig. 3a) led to more available glycerol to be packed with amylose, the DRX behavior of this film was expectable.

In TPS80 and TPS120 the grains were completely gelatinized leading to completed gelatinized material, as can be seen in SEM micrographs (Fig. 3b and c). The diffraction pattern of TPS120 resulted amorphous, whereas TPS80 showed the formation of new

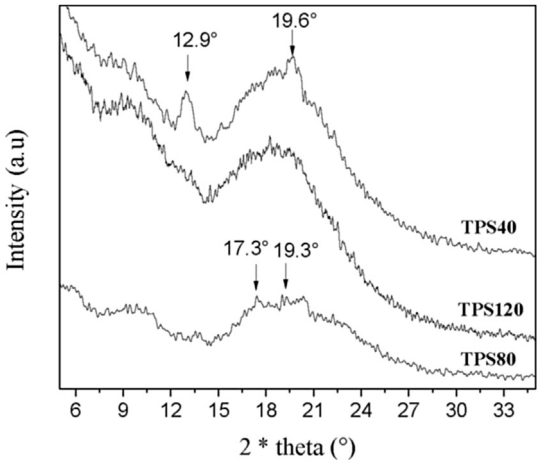

Fig. 5. Representative XRD curves of the different studied films. The curves differ from each other by 2%.

crystal peaks at 2Θ ~17.3° and 19.3°, corresponding to starch retrogradation (Lara & Salcedo, 2016; Seligra, Jaramillo, Famá, & Goyanes, 2016). Retrogradation occurs during storage, and the rate of retrogradation depends strongly on the storage conditions (Farhat, Blanshard, & Mitchell, 2000). Lara (Lara & Salcedo, 2016) demonstrated that starch/glycerol/water systems with partially destroyed grains on their structure did not show retrogradation, while in complete gelatinized systems, amylopectin recrystallization occurred, leading to the appearance of peaks at 17.0° and 19.3° (Lara & Salcedo, 2016). DRX results indicate that retrogradation could occur during the storage of the threads because they were stabilized for 4 weeks, but not in the films because they were tested immediately (stabilized 72 h). Then, due to the presence of non-gelatinized starch grains in the threads processed at 120 rpm, retrogradation after 4 weeks of stabilization occurred more slowly than in the threads at 80 rpm. Therefore, TPS120 showed practically amorphous pattern compared to TPS80. Therefore, TPS120 showed practically amorphous pattern respect to TPS80.

In loss tangent (tan δ) dependence on temperature curve of TPS120, two relaxation processes, one with a well marked temperature peak at around 71 °C, and other less intensity at ~ 10 °C, was observed (Fig. 6). Following the literature, the first transition (T ~ 10 °C) corresponds to the rearrangement of amorphous amylopectin chains in the presence of moisture (García et al., 2009), and the second is attributed to the transition of starch-rich domains.

Several authors reported the relaxation process related to the glass transition of starch-rich domains of starch plasticized films at temperatures in a range of 30–100 °C (García et al., 2009; Madrigal, Sandoval, & Müller, 2011; Morales et al., 2015; Xie et al., 2015).

TPS80 showed similar behavior than TPS120 but with peaks much less marked, being the first almost imperceptible; typical of thermoplastic starch films with the plasticizer homogeneously distributed. The more intense and pronounced transitions in the film processed at 120 rpm indicates that there are lower amount of different relaxation modes, probably due to the less glycerol present in the starch phase in that material, being the starch-starch interactions more dominant.

During starch gelatinization process, the granule structure collapses for the melting of the crystallites and then amylose and amylopectin are partly separated. Shear stress during extrusion may enhance such separation, whereby amylose may be partly leached out of the amylopectin (Liu et al., 2009). Accordingly, while amylose gelatinized (amylose unordered), part of amylopectin cannot still gelatinize (amylopectin crystal). Considering that in the thread processed at 120 rpm broken grains remained (starch did not completely gelatinized), possibly part of amylopectin has be still ungelatinized within the thermoplastic matrix. Once that material was pressed, such amylopectin gelatinized and/or melted, creating glycerol-amylopectin interactions. A scheme of the possible configuration with the presence of glycerol-amylopectin interactions are exposed in Fig. 7.

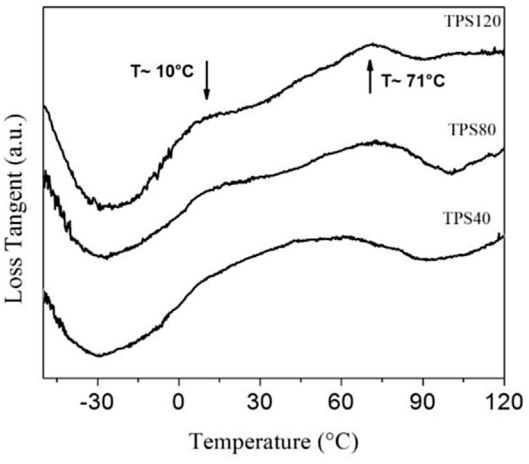

Fig. 6. Representative Loss Tangent curves, as a function of the temperature of TPS40, TPS80 and TPS120. The curves differ from each other by 1%.

The film fabricated at 40 rpm showed a very broad transition between 10 and 60 °C. Taking into account the structure of TPS40 (broken grains in a plasticized matrix with high concentration and non-homogeneously distributed glycerol), the observed transition corresponds to glycerol-starch and is wider by the different mechanisms occurred due to the non-homogenized glycerol distribution. On other hand, a shift to lower temperatures of the peak related to the starch-rich domains of a glycerol-starch material is due to the higher amount of glycerol presented in the plasticized area of TPS40.

Representative stress-strain curves for all films are shown in Fig. 8. All materials exhibited linear visco-elastic range where the stress increases linearly with the strain, followed by a non-linear behavior. Above non-linear zone, each material displayed different behavior. TPS40 showed immediately failure due to the presence of starch grains that act as fissure propagators, avoiding plastic deformation. Films processed at 120 rpm showed a short zone of plastic deformation and then the break, and TPS80 presented more range of plastic region before failure, typical behavior of ductile material.

Young's modulus (E), stress at break (σ_b) and strain at break (ε_b) values are depicted in Table 1. TPS80 presented the lowest values of both modulus and stress at break and higher strain at break than films made at 40 and 120 rpm. TPS40 and TPS120 displayed similar values of modulus and greater than TPS80. In the case of the film extruded at 40 rpm, this fact was expectable taking into account the presence of broken starch grains in that material, which makes that the modulus increase and strain at break significant decrease with respect to TPS80, because starch grains are great fissure propagators. On the other hand, the high storage modulus in TPS120 compared to TPS80 resulted from the strong starch-starch interactions in that film after pressing, as it was explained above from tan δ curves. It is well known that these interactions are stronger than that of starch-glycerol, leading to an increase in the modulus.

Highest water vapor permeability (WVP) value was obtained for TPS40 (Table 2). This result is consistent with the structure of that film. The presence of starch grains and phase separation led to a material with a reduction on both cohesion and homogeneity of the plasticized matrix, provoking preferential paths that facilitates the transfer of water molecules, then, increasing WVP. Water vapor permeability of TPS80 and TPS120 did not show significant differences and they are in accordance with those reported in the literature for plasticized starch films.

Water solubility (S) (Table 2) revealed that TPS40 and TPS80 values did not presented significant differences while the solubility of TPS120 was smaller. As it was explained in experimental section, the mass used of each system was the same. Such mass is formed by both amorphous and crystalline zones in different proportions, as it could be seen in DRX assays. As it is known, crystalline structure is much more difficult to solubilize in water. On the other hand, the solubility of starch-glycerol films is highly dependent of plasticizer concentration, when glycerol content increases, solubility increases too (Hu, Chen, & Gao, 2009). The similar results of the solubility of TPS40 and TPS80 is related to two factors. On a one hand, the smaller amorphous mass of TPS40 compared to TPS80 (see Fig. 5), would trend to decrease. On the other hand, in that amorphous zones the concentration of glycerol is higher, then, larger mass is

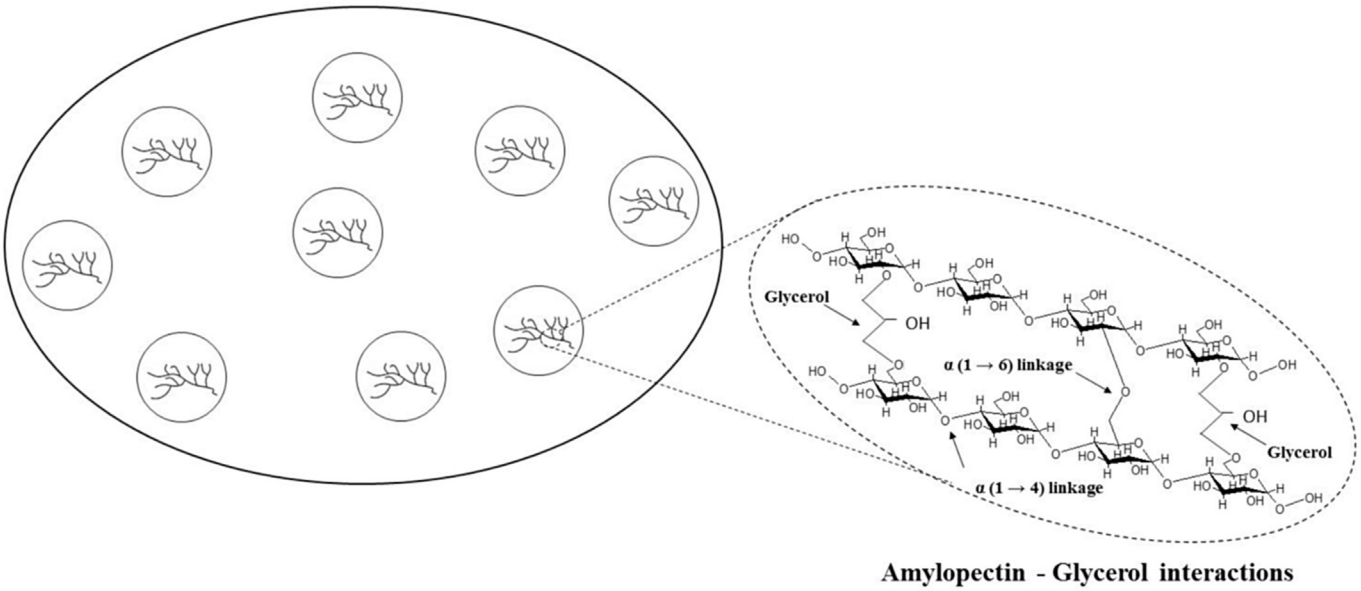

Fig. 7. Scheme of the possible configuration of glycerol-amylopectin interactions in the starch matrix.

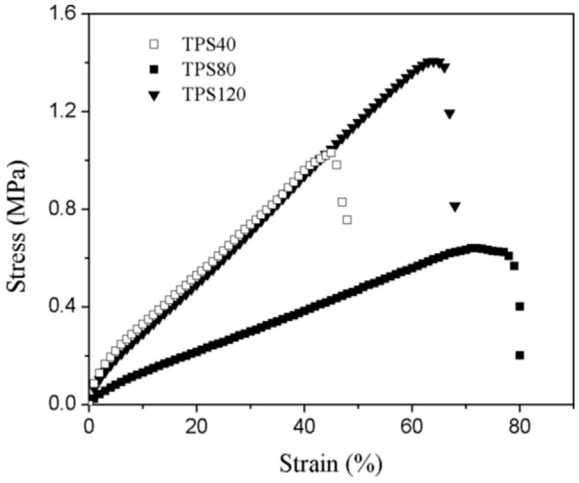

Fig. 8. Representative Stress- Strain curves of the three films developed. The curves differ from each other by 15%.

Table 1
Young's modulus (E), strain at break (ε) and tensile strength (σ) values for the films.

System	E (MPa)	ε (%) [± 5]	σ (MPa)
TPS40	21 ± 2[a]	45	1.0 ± 0.2[b]
TPS80	9 ± 1	78	0.55 ± 0.08
TPS120	21 ± 2[a]	65	1.4 ± 0.2[b]

[a,b] Values with the same letter are not significantly different ($p > 0.05$).

Table 2
Water vapor permeability (WVP) and solubility (S) for the films.

System	WVP (g/m s Pa) x 10^{-10}	S (%)
TPS40	12.0 ± 1.2	31 ± 3[b]
TPS80	6.1 ± 0.7[a]	32 ± 4[b]
TPS120	6.9 ± 0.8[a]	25 ± 2

[a,b] Values with the same letter are not significantly different ($p > 0.05$).

possible to solubilize. TPS80 has greater portion of amorphous mass than TPS40 but least of it was solubilized due to the lower glycerol concentration presented in that part.

Beyond similar values of solubility of TPS120 and TPS80 comparing DRX patterns was expectable, the strong starch-starch interactions of the film prepared at 120 rpm make the material more difficult to dissolve in water because this type of interactions are more difficult to break than that of starch-glycerol.

5. Conclusions

The effect of the screw speed on the extrusion process of thermoplastic starch materials was determinant in their structure and physicochemical properties, and therefore in their possible applications in food packaging industries. Starch-glycerol-water mixes were extruded at 40, 80 and 120 rpm, maintaining the temperature profile and all other process conditions. The slowest screw speed condition lead to a material with a high density of non gelatinized broken grains and inhomogeneity in glycerol distribution, which resulted in high cristallinity and resistance to break but with a tendency to break at lower deformations. Extrusion at screw speed of 80 rpm is suitable to obtain homogeneous thermoplastic starch materials in both forms, threads and films, but with faster starch retrogradation. Finally, if it is desired amorphous starch thermoplastic films with greater modulus, tensile strength and slower starch retrogradation, the best option is to use 120 rpm.

Funding

This work was supported by the following organizations: Agencia Nacional de Promoción Científica y Tecnológica [ANPCyT 2012-1093], Consejo Nacional de Investigaciones Científicas y Técnicas [CONICET PIP 2014–2016 11220120100508CO, 2014–2016], and Universidad de Buenos Aires [UBACYT 2014–2017 20020130100495BA, 2014–2017].

References

Alam, M. S., Pathania, S., & Sharma, A. (2016). Optimization of the extrusion process for development of high fibre soybean-rice ready-to-eat snacks using carrot

pomace and cauliflower trimmings. *LWT-Food Science and Technology, 74*, 135–144.
Bashir, K., Swer, T. L., Prakash, K. S., & Aggarwal, M. (2017). Physico-chemical and functional properties of gamma irradiated whole wheat flour and starch. *LWT-Food Science and Technology, 76*, 131–139.
Borries-Medrano, E., Jaime-Fonseca, M. R., & Aguilar-Mendez, M. A. (2016). Starch-guar gum extrudates: Microstructure, physicochemical properties and in-vitro digestion. *Food Chemistry, 194*, 891–899.
Brand-Williams, W., Cuvelier, M. E., & Berset, C. (1995). Use of a free radical method to evaluate antioxidant activity. *LWT-Food Science and Technology, 28*(1), 25–30.
Campos-Requena, V. H., Rivas, B. L., Pérez, M. A., Garrido-Miranda, K. A., & Pereira, E. D. (2015). Polymer/clay nanocomposite films as active packaging material: Modeling of antimicrobial release. *European Polymer Journal, 71*, 461–475.
Chaudhary, A. L., Miler, M., Torley, P. J., Sopade, P. A., & Halley, P. J. (2008). Amylose content and chemical modification effects on the extrusion of thermoplastic starch from maize. *Carbohydrate Polymers, 74*(4), 907–913.
Deng, J., Li, K., Harkin-Jones, E., Price, M., Karnachi, N., Kelly, A., et al. (2014). Energy monitoring and quality control of a single screw extruder. *Applied Energy, 113*, 1775–1785.
Famá, L., Bittante, A. M. B., Sobral, P. J., Goyanes, S., & Gerschenson, L. N. (2010). Garlic powder and wheat bran as fillers: Their effect on the physicochemical properties of edible biocomposites. *Materials Science and Engineering: C, 30*(6), 853–859.
Famá, L., Goyanes, S., & Gerschenson, L. (2007). Influence of storage time at room temperature on the physicochemical properties of cassava starch films. *Carbohydrate Polymers, 70*, 265–273.
Famá, L. M., Pettarin, V., Goyanes, S. N., & Bernal, C. R. (2011). Starch/multi-walled carbon nanotubes composites with improved mechanical properties. *Carbohydrate Polymers, 83*(3), 1226–1231.
Famá, L., Rojas, A. M., Goyanes, S., & Gerschenson, L. (2005). Mechanical properties of tapioca-starch edible films containing sorbates. *LWT-food Science and Technology, 38*(6), 631–639.
Famá, L., Rojo, P. G., Bernal, C., & Goyanes, S. (2012). Biodegradable starch based nanocomposites with low water vapor permeability and high storage modulus. *Carbohydrate Polymers, 87*(3), 1989–1993.
Farhat, I., Blanshard, J., & Mitchell, J. (2000). The retrogradation of waxy maize starch extrudates: Effects of storage temperature and water content. *Biopolymers, 53*(5), 411–422.
García, N. L., Famá, L., Dufresne, A., Aranguren, M., & Goyanes, S. (2009). A comparison between the physico-chemical properties of tuber and cereal starches. *Food Research International, 42*(8), 976–982.
García, N., Famá, L., D'Accorso, N., & Goyanes, S. (2015). Biodegradable starch nanocomposites. In V. K. Thakur, & M. K. Thakur (Eds.), *Eco-friendly polymer nanocomposites* (pp. 17–77). India: Springer.
Ghanbarzadeh, B., & Almasi, H. (2013). Biodegradable polymers. In R. Chamy, & F. Rosenkranz (Eds.), *Biodegradation – life of science* (pp. 141–186). Croatia: InTech Publications.
Gilfillan, W. N., Moghaddam, L., Bartley, J., & Doherty, W. O. S. (2016). Thermal extrusion of starch film with alcohol. *Journal of Food Engineering, 170*, 92–99.
Godavarti, S., & Karwe, M. (1997). Determination of specific mechanical energy distribution on a twin-screw extruder. *Journal of Agricultural Engineering Research, 67*(4), 277–287.
González-Seligra, P., Eloy-Moura, L., Famá, L., Druzian, J. I., & Goyanes, S. (2016). Influence of incorporation of starch nanoparticles in PBAT/TPS composite films. *Polymer International, 65*, 938–945.
Goudarzi, V., Shahabi-Ghahfarrokhi, I., & Babaei-Ghazvini, A. (2017). Preparation of ecofriendly UV-protective food packaging material by starch/TiO 2 bio-nanocomposite: Characterization. *International Journal of Biological Macromolecules, 95*, 306–313.
Graaf, R. A., Karman, A. P., & Janssen, L. P. (2003). Material properties and glass transition temperatures of different thermoplastic starches after extrusion processing. *Starch-Stärke, 55*(2), 80–86.
Gutiérrez, T. J., Morales, N. J., Pérez, E., Tapia, M. S., & Famá, L. (2015). Physico-chemical properties of edible films derived from native and phosphated cush-cush yam and cassava starches. *Food Packaging and Shelf Life, 3*, 1–8.
Hietala, M., Mathew, A. P., & Oksman, K. (2013). Bionanocomposites of thermoplastic starch and cellulose nanofibers manufactured using twin-screw extrusion. *European Polymer Journal, 49*(4), 950–956.
Homayouni, H., Kavoosi, G., & Nassiri, S. M. (2017). Physicochemical, antioxidant and antibacterial properties of dispersion made from tapioca and gelatinized tapioca starch incorporated with carvacrol. *LWT-Food Science and Technology, 77*, 503–509.
Hu, G., Chen, J., & Gao, J. (2009). Preparation and characteristics of oxidized potato starch films. *Carbohydrate Polymers, 76*(2), 291–298.
Jaramillo, C. M., Gutiérrez, T. J., Goyanes, S., Bernal, C., & Famá, L. (2016). Biodegradability and plasticizing effect of yerba mate extract on cassava starch edible films. *Carbohydrate Polymers, 151*, 150–159.
Kelly, A. L., Brown, E. C., & Coates, P. D. (2006). The effect of screw geometry on melt temperature profile in single screw extrusion. *Polymer Engineering & Science, 46*(12), 1706–1714.
Kibar, E. A. A., & Us, F. (2013). Thermal, mechanical and water adsorption properties of corn starch–carboxymethylcellulose/methylcellulose biodegradable films. *Journal of Food Engineering, 114*(1), 123–131.
Kruiskamp, P., Smits, A., Van Soest, J., & Vliegenthart, J. (2001). The influence of plasticiser on molecular organisation in dry amylopectin measured by differential scanning calorimetry and solid state nuclear magnetic resonance spectroscopy. *Journal of Industrial Microbiology and Biotechnology, 26*(1-2), 90–93.
Lai, L., & Kokini, J. (1990). The effect of extrusion operating conditions on the on-line apparent viscosity of 98% Amylopectin (Amioca) and 70% Amylose (Hylon 7) corn starches during extrusion. *Journal of Rheology, 34*(8), 1245–1266.
Lai, L., & Kokini, J. (1991). Physicochemical changes and rheological properties of starch during extrusion. (A review). *Biotechnology Progress, 7*(3), 251–266.
Lara, S. C., & Salcedo, F. (2016). Gelatinization and retrogradation phenomena in starch/montmorillonite nanocomposites plasticized with different glycerol/water ratios. *Carbohydrate Polymers, 151*, 206–212.
Li, M., Liu, P., Zou, W., Yu, L., Xie, F., Pu, H., et al. (2011). Extrusion processing and characterization of edible starch films with different amylose contents. *Journal of Food Engineering, 106*(1), 95–101.
Liu, H., Xie, F., Yu, L., Chen, L., & Li, L. (2009). Thermal processing of starch-based polymers. *Progress in Polymer Science, 34*(12), 1348–1368.
Madrigal, L., Sandoval, A. J., & Müller, A. J. (2011). Effects of corn oil on glass transition temperatures of cassava starch. *Carbohydrate Polymers, 85*(4), 875–884.
Maizura, M., Fazilah, A., Norziah, M. H., & Karim, A. A. (2007). Antibacterial activity and mechanical properties of partially hydrolyzed sago starch-alginate edible film containing lemon grass oil. *Journal of Food Science, 72*(6), 324–330.
Morales, N. J., Candal, R., Famá, L., Goyanes, S., & Rubiolo, G. H. (2015). Improving the physical properties of starch using a new kind of water dispersible nano-hybrid reinforcement. *Carbohydrate Polymers, 127*, 291–299.
Moreno, O., Pastor, C., Muller, J., Atarés, L., González, C., & Chiralt, A. (2014). Physical and bioactive properties of corn starch–Buttermilk edible films. *Journal of Food Engineering, 141*, 27–36.
Oniszczuk, T., Wójtowicz, A., Oniszczuk, A., Mitrus, M., Combrzyński, M., Kręcisz, M., et al. (2015). Effect of processing conditions on selected properties of starch-based biopolymers. *Agriculture and Agricultural Science Procedia, 7*, 192–197.
Piñeros-Hernandez, D., Medina-Jaramillo, C., López-Córdoba, A., & Goyanes, S. (2017). Edible cassava starch films carrying rosemary antioxidant extracts for potential use as active food packaging. *Food Hydrocolloids, 63*, 488–495.
Rodríguez-Castellanos, W., Martínez-Bustos, F., Rodrigue, D., & Trujillo-Barragán, M. (2015). Extrusion blow molding of a starch–gelatin polymer matrix reinforced with cellulose. *European Polymer Journal, 73*, 335–343.
Rosa, D., Carvalho, C., Gaboardi, F., Rezende, M., Tavares, M., Petro, M., et al. (2008). Evaluation of enzymatic degradation based on the quantification of glucose in thermoplastic starch and its characterization by mechanical and morphological properties and NMR measurements. *Polymer Testing, 27*(7), 827–834.
Saiah, R., Sreekumar, P. A., Gopalakrishnan, P., Leblanc, N., Gattin, R., & Saiter, J. M. (2009). Fabrication and characterization of 100% green composite: Thermoplastic based on wheat flour reinforced by flax fibers. *Polymer Composites, 30*(11).
Seligra, P. G., Jaramillo, C. M., Famá, L., & Goyanes, S. (2016). Biodegradable and non-retrogradable eco-films based on starch–glycerol with citric acid as cross-linking agent. *Carbohydrate Polymers, 138*, 66–74.
Van Soest, J. J., Hulleman, S., De Wit, D., & Vliegenthart, J. (1996). Crystallinity in starch bioplastics. *Industrial Crops and Products, 5*(1), 11–22.
Wang, Y. Y., & Ryu, G.-H. (2013). Physicochemical and antioxidant properties of extruded corn grits with corn fiber by CO2 injection extrusion process. *Journal of Cereal Science, 58*(1), 110–116.
Wang, K., Wang, W., Ye, R., Liu, A., Xiao, J., Liu, Y., et al. (2017). Mechanical properties and solubility in water of corn starch-collagen composite films: Effect of starch type and concentrations. *Food Chemistry, 216*, 209–216.
Xie, M., Duan, Y., Li, F., Wang, X., Cui, X., Bacha, U., et al. (2016). Preparation and characterization of modified and functional starch (hexadecyl corboxymethyl starch) ether using reactive extrusion. *Starch-Stärke, 68*, 1–9.
Xie, F., Flanagan, B. M., Li, M., Truss, R. W., Halley, P. J., Gidley, M. J., et al. (2015). Characteristics of starch-based films with different amylose contents plasticised by 1-ethyl-3-methylimidazolium acetate. *Carbohydrate Polymers, 122*, 160–168.
Zepon, K. M., Vieira, L. F., Soldi, V., Salmoria, G. V., & Kanis, L. A. (2013). Influence of process parameters on microstructure and mechanical properties of starch-cellulose acetate/silver sulfadiazine matrices prepared by melt extrusion. *Polymer Testing, 32*(6), 1123–1127.